

An MHD Model For Magnetar Giant Flares

Y. Meng^{1,2}, J. Lin¹, L. Zhang³, K. K. Reeves⁴, Q.S. Zhang^{1,5}, and F. Yuan⁶

mengy@ynao.ac.cn, jlin@ynao.ac.cn

Received _____; accepted _____

¹Yunnan Observatory, Chinese Academy of Sciences, P. O. Box 110, Kunming, Yunnan 650011, China.

²University of Chinese Academy of Sciences, Beijing 100039, China.

³Department of Physics, Yunnan University, Kunming, Yunnan 650091, China

⁴Harvard-Smithsonian Center for Astrophysics, 60 Garden Street, Cambridge, MA 02138, USA

⁵Key Laboratory for the Structure and Evolution of Celestial Objects, Yunnan Astronomical Observatory, Chinese Academy of Sciences, Kunming, Yunnan 650011, China

⁶Key Laboratory for Research in Galaxies and Cosmology, Shanghai Astronomical Observatory, Chinese Academy of Sciences, 80 Nandan Road, Shanghai 200030, China

ABSTRACT

Giant flares on soft gamma-ray repeaters that are thought to take place on magnetars release enormous energy in a short time interval. Their power can be explained by catastrophic instabilities occurring in the magnetic field configuration and the subsequent magnetic reconnection. By analogy with the coronal mass ejection (CME) events on the Sun, we develop a theoretical model via an analytic approach for magnetar giant flares. In this model, the rotation and/or displacement of the crust causes the field to twist and deform, leading to flux rope formation in the magnetosphere and energy accumulation in the related configuration. When the energy and helicity stored in the configuration reach a threshold, the system loses its equilibrium, the flux rope is ejected outward in a catastrophic way, and magnetic reconnection helps the catastrophe develop to a plausible eruption. By taking SGR 1806 - 20 as an example, we calculate the free magnetic energy released in such an eruptive process and find that it is more than 10^{47} ergs, which is enough to power a giant flare. The released free magnetic energy is converted into radiative energy, kinetic energy and gravitational energy of the flux rope. We calculated the light curves of the eruptive processes for the giant flares of SGR 1806 - 20, SGR 0526-66 and SGR 1900+14, and compared them with the observational data. The calculated light curves are in good agreement with the observed light curves of giant flares.

Subject headings: instabilities - MHD - magnetic reconnection - stars: individual(SGR1806-20) - stars: magnetic fields - stars: neutron -stars: flare

1. Introduction

Soft gamma repeaters (SGRs) and anomalous X-ray pulsars (AXPs) are believed to be magnetars - a small class of spinning neutron stars with ultra-strong magnetic fields ($B \geq 10^{15}$ G), which are thought to result from dynamo action during supernova collapse (Duncan & Thompson 1992; Kouveliotou et al. 1998; Thompson & Murray 2001; Lyutikov 2003; Harding & Lai 2006). The emission from a magnetar is powered by the dissipation of non-potential (current-carrying) magnetic fields in the magnetosphere (Duncan & Thompson 1992; Thompson & Duncan 1996; Thompson et al. 2002; Lyutikov 2006). Both SGRs and AXPs show quiescent persistent X-ray and repeated soft gamma-ray emissions (Mereghetti et al. 2004). Extremely rarely, an SGR produces a giant flare with enormous energy ($\simeq 10^{44} - 10^{47}$ erg) and long burst duration. These exceptionally powerful outbursts begin with a very short (~ 0.2 s) spike of γ -rays containing most of the flare energy and the spike is followed by a pulsating tail lasting a few hundreds of seconds (Hurley et al. 2005).

So far, three SGRs have been reported to produce giant flares (Mazets et al. 1979; Hurley et al. 1999, 2005). They include SGR 0526-66 on 5 March 1979 (Mazets et al. 1979), SGR 1900+ 14 on 27 August 1998 (Hurley et al. 1999; Kouveliotou et al. 1999; Vrba et al. 2000), and SGR 1806-20 on 27 December 2004 (Hurley et al. 2005; Palmer et al. 2005). The giant flare from SGR 1806- 20 was much more luminous than the other two events (Hurley et al. 2005; Palmer et al. 2005). Its initial γ -ray spike released an energy of $\sim 10^{46}$ erg within ~ 0.2 s, and its rising and falling times were $\tau_{rise} \leq 1$ ms and $\tau_{fall} \approx 65$ ms, respectively. The main spike was followed by a tail with ~ 50 pulsations of high-amplitude at the rotation period (7.56s) of SGR 1806 - 20 (Hurley et al. 2005; Palmer et al. 2005).

Although the energy of a magnetar outburst is widely believed to come from the star's magnetic field, details of the physical process in which the magnetic energy is stored and released remain unknown. So far, two models of giant flares of SGRs exist, which depend on the location

where the magnetic energy is stored prior to the eruption: one assumes that the energy is stored in the crust of the neutron star (crust model) and the other one assumes that the storage occurs in the magnetosphere (magnetosphere model). In the crust model, a giant flare is caused by a sudden untwisting of the internal magnetic field (Thompson & Duncan 1995, 2001; Lyutikov 2006). Subsequently, a large and quick rotational displacement on the time-scale of a flare leads to the giant flare. Alternatively, in the magnetosphere model, the magnetic energy is slowly stored in the magnetosphere on time scales much longer than that of the giant flare itself, until the system reaches a critical state at which the equilibrium becomes unstable. Then further evolution in the system occurs and leads to flares, in analogy with solar flares and coronal mass ejections (CMEs) taking place in the solar atmosphere (Lyutikov 2006). Observations of the giant flare from SGR 1806-20 on 27 December 2004 showed that it lasted a very short rise time, ~ 0.25 ms (Palmer et al. 2005). This time interval of the eruption is short compared to the time-scale required for the crust model (Thompson & Duncan 1995; Lyutikov 2003, 2006). Therefore, at least for the SGR 1806 - 20, the time-scale of the crust model is too long to account for the triggering and early stage evolution of the event.

The magnetosphere model based on an analogy with solar CMEs was proposed by Lyutikov (2006). In this model, the magnetic energy released during a giant flare is built up slowly in the magnetosphere, not in the crust of the neutron star. Although the energy storage process is gradual and long, the energy release takes place within a very short timescale in a dynamical fashion (Lyutikov 2006). Transition from slow to fast evolution constitutes the catastrophe that is similar to what happens in solar flares and CMEs (see Forbes & Isenberg 1991; Isenberg et al. 1993). Moreover, the profile of the light curve of solar-flare/ CME events resembles that of magnetar giant flares. Both of them have an impulsive phase and a tail emission. Similar morphology and characteristics between magnetar giant flares and solar-flare/ CME events indicate the operation of a common physical mechanism. Therefore, solar flares and CMEs give an important prototype context for magnetar giant flares. Masada et al. (2010) constructed a theoretical model for a

magnetar giant flares based on the solar-flare/ CMEs model. They described magnetar giant flare using a magnetic reconnection model of a solar flare proposed by Shibata & Yokoyama (1999) while taking account of chromospheric evaporation. In their work, the preflare activity produces a baryon-rich prominence. Then the prominence erupts as a result of magnetic reconnection, and the eruption constitutes the origin of the observed radio-emitting ejecta associated with the giant flare from SGR 1806- 20 (Taylor et al. 2005; Cameron et al. 2005; Gaensler et al. 2005; Masada et al. 2010). A giant flare should be induced as the final outcome of prominence eruption accompanied by large-scale field reconfigurations (Masada et al. 2010).

Numerical simulations have also been performed in order to construct an MHD model for a magnetar giant flare. Parfrey et al. (2012a,b, 2013) presented the simulations of evolving strongly twisted magnetic fields in the magnetar magnetosphere. Their results showed that slow shearing of the magnetar crust leads to a series of magnetospheric expansion and reconnection events, corresponding to X-ray flares and bursts. They studied the relationship between the increasing twist and the spindown rate of the star, and concluded that the observed giant flares could be caused by the sudden opening of large amounts of overtwisted magnetic flux, resulting in an abrupt increase in spin period.

Motivated by CME studies, Yu (2011) constructed a general relativistic model of non-rotating magnetars, which simulated how the magnetic field could possess enough energy to overcome the Aly-Sturrock energy constraint and open up. Furthermore, by taking into account the possible flux injections and crust motions, Yu (2012) built a force-free magnetosphere model with a flux rope suspended in the magnetosphere and investigated the catastrophic behavior of the flux rope in a background with multi-polar magnetic field. In this model, a gradual process leads to a sudden release of the magnetosphere energy on a dynamical timescale (Yu 2012). Therefore, the existing catastrophe model for solar eruptions could be a good template for constructing a theoretical model for magnetar giant flares.

The initiation and development of magnetar giant flares have been extensively studied and several models have been suggested (Thompson & Duncan 1995, 2001; Lyutikov 2006; Masada et al. 2010; Yu 2011, 2012). But the origin and development of these giant flares remains unclear. The detailed physical process of the magnetic energy storage and release is still an open question. In this work, we consider relativistic effects and construct a magnetohydrodynamical (MHD) model for magnetar giant flares in the framework of the CME catastrophe model (Lin & Forbes 2000), then duplicate the dynamical process of the giant flares produced by SGR 1806-20. We describe our model in next section. Results of calculations and comparisons with observations are in Section 3. Finally, we discuss these results and summarize this work in Section 4.

2. Model Description

In the framework of the catastrophe model of solar eruptions, the evolution in the system that eventually leads to a plausible eruption includes two stages and a triggering process that initiates the second stage. In the first stage, the magnetic energy is gradually stored in the coronal magnetic field in response to a motion or change inside the star, and the stored energy is quickly released in the second stage. The second stage follows the first one via a triggering process, which is also known as the loss of the equilibrium. This process could be either ideal or non-ideal MHD depending on the fashion of the system evolution or detailed structure in the magnetic field involved (e.g., see discussions of Forbes & Isenberg 1991; Lin et al. 2003). But magnetic reconnection is crucial for the energy released to produce the flare (Parker 1963; Petschek 1964) and to allow the CME to propagate smoothly (Lin & Forbes 2000).

Figure 1 shows a typical eruptive event or process (or CME) in the solar magnetic atmosphere (the original figure was obtained from the SDO website: <http://sdo.gsfc.nasa.gov/>). In this process, because of the instability, the magnetic configuration including a large amount of high temperature

plasma is ejected outward from the solar surface, associated with intensive electromagnetic radiation (namely the well-known solar flare) and energetic particles (e.g., see also Švestka 1976; Priest & Forbes 2002). Since the highly ionized plasma and the magnetic field are frozen to one another (Priest 1982), the plasma is confined in the nearby magnetic configuration. Therefore, we are able to infer magnetic structure and some internal details according to the level of concentration or spatial distributions of the ambient plasma, which is shown as different bright or dark features in the picture displayed in Figure 1, although we cannot see the magnetic structure itself directly.

The complex global and local structures in the magnetic configuration shown in Figure 1 indicate high non-potentiality of the associated magnetic field and strong interactions between the magnetic field and the electric current in that region. Hence, as a result, enough magnetic free energy (i.e., the difference between the total magnetic energy in a system and the magnetic potential energy in the same system) prior to the eruption can be stored to drive the eruption. A sketch for qualitatively describing the disrupting magnetic field is inserted in the figure, with more details being specified in Figure 2: the closed circles in the middle represents the core of the CME, the ambient curves represent the magnetic field lines associated with the CME. More explanations for mathematical notes will be given later. Since it is surrounded by strong magnetic fields and plasma, a magnetar is quite likely to possess similar complex magnetic configurations in its magnetosphere and eventually to produce energetic eruptions, which must be, of course, much more powerful than those occurring on the Sun.

We note that the driver of the energy transport occurring in the solar atmosphere is the motion of the dense plasma in the photosphere, but the crust of the magnetar is solid and might not be able to move as the mass in the photosphere. However, crust cracking could take place on the magnetar from time to time (see Ruderman 1991a,b,c). The surface magnetic field of a spin-down crust-cracking neutron star might break up into large surface patches (platelets) which

would move apart from one another (Ruderman 1991c). On the other hand, the Lorentz force due to the strong magnetic field acting on the crust could result in the build up of stress, and further causes pieces of the broken crust to rotate on the equipotential surface as the stress acting on the lattice exceeds a critical value (Lyutikov 2006). This processes eventually leads to the storage of magnetic stress and thus energy in the magnetosphere.

Therefore, the energy driving the giant flare on the magnetar could be transported from the inside of the magnetar via a reasonable mechanism, and then stored in the magnetosphere before the eruption, although the basic driver of energy storage is somewhat different from that on the Sun. More effects of the footpoint motions of the magnetic field on the magnetar were also studied by Thompson & Duncan (1995). They studied the effect of a sudden shift in footpoints of the magnetospheric field (see Figure 1.(a) in their paper) on the energy release. The effect of crust motions on the release of magnetic energy was also studied in the numerical simulations by Yu (2012).

Lin & Forbes (2000) developed an analytic model of solar eruptions (Figure 2) that explains the mutual impact of magnetic reconnection and the CME acceleration on each other. Magnetic reconnection plays very important role in the eruption. It helps to eject the flux rope successfully and to form a CME; it produces flare loops, flare ribbons and the rapid expanding CME bubbles (Lin et al. 2004; Lin & Soon 2004); and its non-ideal MHD properties lead to a natural avoidance of the Aly-Sturrock paradox (Aly 1991; Sturrock 1991), which was first noticed by Aly (1984), such that a purely ideal MHD process in the force-free environment could not fully open the closed magnetic field to produce CMEs (Forbes 2000; Klimchuk 2001; Lin et al. 2003).

2.1. Equations For Basic Magnetic Configuration

In this work, we build an MHD model for magnetar giant flares based on a solar flare/CME model, including the effects of special relativity. Since the magnetars that have so far been observed have a very slow rotation, and the time scale of the main spike of the magnetar giant flare is short compared to their rotation periods, we ignore rotation effects on the eruption in our model. But we understand that the rotation should play an important role in the first stage. We now elaborate the possible magnetic configuration that includes a flux rope floating in the magnetosphere and may give an eruption eventually. The precursor of a giant flare could be closely connected to the pre-existence of the flux rope that includes twisted magnetic field (Götz et al. 2007; Gill & Heyl 2010; Yu 2012).

We note here that our model is plane symmetric instead of axial-symmetric, and the evolutionary behavior of the disrupted magnetic field revealed in this work yields valuable and important observational consequences. But we understand as well that our calculation is performed in two-dimensions. The cartoon in Figure 2 could be considered as the cross section of a three dimensional configuration, which includes a flux rope with two ends anchored to the crust of the central star such as those shown in Figure 1. Therefore, the effect of the anchorage of both the flux rope ends and the expelling force due to the curvature of the flux rope (see also Lin et al. 1998, 2002; Isenberg & Forbes 2007) in reality are not included in our calculations. Furthermore, the impact of the centrifugal force due to the spin of the neutron star on the evolution of the disrupting magnetic configuration is not included, either.

Generally, the anchorage tends to prevent the outward motion of the flux rope, and the other two forces play the opposite role in governing the evolution of the system. The expelling and attracting forces acting on the flux rope might counterbalance one another and show no net effect on the system evolution eventually. But details need to be studied carefully, which would constitute the main content of our work in the future in a more realistic environment.

According to the widely accepted physical scenario of the magnetar (Duncan & Thompson 1992; Kouveliotou et al. 1998; Thompson & Murray 2001; Lyutikov 2003; Harding & Lai 2006), the magnetosphere of a slowly rotating neutron star includes a strong magnetic field, and the magnetic field is rooted in the crust of the star. The rotation and/or the displacement of the crust cause the field to twist and deform leading to flux rope formation and energy accumulation in the magnetosphere.

Gravity and magnetic forces in this configuration is acting on the flux rope (Lin et al. 2006). The gas pressure is much smaller than the magnetic forces, so it is negligible in this model. Prior to the loss of equilibrium, the evolution in the system is ideal and magnetic reconnection does not take place in the magnetosphere; and the gradual evolution in the system in response to the slowly varying boundary conditions at the magnetar surface eventually causes the loss of equilibrium in the configuration to occur in a catastrophic fashion.

During this process, the magnetic energy is accumulating slowly until it reaches a critical value as shown in Figure 3, where the flux rope is at a critical position, and the catastrophic loss of equilibrium occurs and the flux rope is thrust outward. Following the loss of equilibrium, the flux rope is thrust outward and its motion is governed by

$$m\gamma^3 \frac{d^2 h}{dt^2} = \frac{1}{c} |\mathbf{I} \times \mathbf{B}_{ext}| - F_g \quad (1)$$

to the first order of approximation, where m is the total mass inside the flux rope per unit length, $\gamma = 1/\sqrt{1 - v^2/c^2}$ is the Lorentz factor, h is the height of the flux rope from the magnetar surface, \mathbf{I} is the total electric current intensity flowing inside the flux rope, \mathbf{B}_{ext} is the total external magnetic field measured at the center of the flux rope, and F_g is the gravitational force acting on the mass inside the flux rope (see Appendix for details).

In zeroth-order approximation, the following equations hold (see Lin & Forbes 2000, for details):

$$\mathbf{j} \times \mathbf{B} = 0, \quad (2)$$

$$\mathbf{j} = \frac{c}{4\pi} \nabla \times \mathbf{B}, \quad (3)$$

where \mathbf{j} and \mathbf{B} are the electric current density and the magnetic field in the system, respectively. In the Cartesian coordinate system (x, y) , the x -axis is on the star surface and y -axis points upward (see also Figure 2). Solving equations (2) and (3) gives the description of the force-free magnetic field in the system (Reeves & Forbes 2005)

$$B(\zeta) = \frac{2iA_0\lambda(h^2 + \lambda^2)\sqrt{(\zeta^2 + p^2)(\zeta^2 + q^2)}}{\pi(\zeta^2 - \lambda^2)(\zeta^2 + h^2)\sqrt{(\lambda^2 + p^2)(\lambda^2 + q^2)}}, \quad (4)$$

where $\zeta = x + iy$, $A_0 = B_0\pi\lambda_0$ is the source field strength and $B_0 = 2I_0/(c\lambda_0) \sim 10^{15}$ G is the magnetic field strength on the surface of the magnetar. The corresponding vector potential function $A(\zeta)$ is as follows:

$$\begin{aligned} A(\zeta) &= - \int B(\zeta)d\zeta \\ &= \frac{2iA_0\lambda p^2}{\pi q\sqrt{(\lambda^2 + p^2)(\lambda^2 + q^2)}} \left\{ \left(1 + \frac{q^2}{\lambda^2}\right) \Pi \left[\tan^{-1} \left(\frac{\zeta}{p} \right), 1 + \frac{p^2}{\lambda^2}, \frac{\sqrt{q^2 - p^2}}{q} \right] \right. \\ &\quad \left. + \left(\frac{q^2}{h^2} - 1 \right) \Pi \left[\tan^{-1} \left(\frac{\zeta}{p} \right), 1 - \frac{p^2}{h^2}, \frac{\sqrt{q^2 - p^2}}{q} \right] \right\}, \quad (5) \end{aligned}$$

where Π is the incomplete elliptic integral of the third kind. According to Lin & Forbes (2000), the current in the flux rope is:

$$I = \frac{c\lambda A_0}{2\pi h} \frac{\sqrt{(h^2 - p^2)(h^2 - q^2)}}{\sqrt{(\lambda^2 + p^2)(\lambda^2 + q^2)}}. \quad (6)$$

2.2. Energetics

The law of the energy conservation determines the total energy in the system at a given time that reads as (see also Reeves 2006)

$$W_{mag} + W_{KE} + W_{EM} + W_{gra} = W_0, \quad (7)$$

where W_{mag} , W_{EM} , W_{KE} , W_{gra} and W_0 are the free magnetic energy, the radiative energy, the kinetic energy of the flux rope, the gravitational potential energy and the initial total energy (a constant) in the system, respectively. Then, we have

$$\frac{d}{dt}(W_{mag} + W_{KE} + W_{EM} + W_{gra}) = 0. \quad (8)$$

From Equation (1), we find that the power related to the kinetic energy is given by

$$\begin{aligned} \frac{dW_{KE}}{dt} &= \frac{d[m_0(\gamma - 1)c^2]}{dt} \\ &= m_0\gamma^3\dot{h}\frac{d^2h}{dt^2} \\ &= \frac{IB_{ext}\dot{h}}{c} - \frac{GM_{NS}\gamma m_0}{(R_0 + h)^2}\dot{h} \\ &= \frac{B_0^2\lambda^4}{8hL_{PQ}^2} \left[\frac{H_{PQ}^2}{2h^2} - \frac{(p^2 + \lambda^2)(h^2 - q^2) + (q^2 + \lambda^2)(h^2 - p^2)}{h^2 + \lambda^2} \right] \dot{h} \\ &\quad - \frac{GM_{NS}\gamma m_0}{(R_0 + h)^2}\dot{h}, \end{aligned} \quad (9)$$

where $H_{PQ} = \sqrt{(h^2 - p^2)(h^2 - q^2)}$, $L_{PQ} = \sqrt{(\lambda^2 + p^2)(\lambda^2 + q^2)}$, $G = 6.67 \times 10^8 \text{ cm}^3 \text{ g}^{-1} \text{ s}^{-2}$ is the gravitational constant, $M_{NS} \sim M_\odot \approx 1.989 \times 10^{33} \text{ g}$ is the mass of neutron star, $m_0 = 10^{20} \text{ g cm}^{-1}$ is the total mass per unit length inside the flux rope. And q , p and h are functions of time.

The impact of the magnetic field on the motion of the flux rope is epitomized by the magnetic compression [the first term in the square bracket at the right hand side of the last equation in (9)] and the magnetic tension [the second term in the square bracket at the right hand side of the last equation in (9)]. Generally, the magnetic compression results from the magnetic field lines between the magnetar surface and the flux rope, which tends to push the flux rope away from the central star; and the magnetic tension is produced by the magnetic field lines overlying the flux rope with two ends anchored to the surface of the central star (see also Figure 10 of Lin et al. 2003). The magnetic field in the solar corona, in fact, dominates the plasma as well, and it plays the same role in driving the solar eruption as in the case of the magnetar giant flare. The last term

in the last equation of (9) comes from the gravity of the mass in the ejecta. The loss of equilibrium in the system takes place as the balance among these forces ceases to exist, and the flux rope is thrust outward with its motion being governed by equation (1) or (9). The relativistic effect on the motion of the flux rope in this process is indicated by the Lorentz factor appearing in the relevant equations.

The power associated with the radiative energy is given by (Reeves 2006)

$$\begin{aligned} \frac{dW_{EM}}{dt} &= S(t) \\ &= \frac{c}{2\pi} E_z(t) \int_{p(t)}^{q(t)} B_y(0, y, t) dy, \end{aligned} \quad (10)$$

where $E_z(t)$ is the electric field in the reconnection region induced in the reconnection process (see details given by Forbes & Lin 2000; Lin & Forbes 2000), the magnetic field along the current sheet $B_y(0, y, t)$ is determined by equation (4) with $x = 0$, q and p are the top and the bottom tips of the current sheet, respectively, as shown in Figure 2. Here the product of the electric field E_z and the magnetic field B_y gives the Poynting flux that describes the electromagnetic energy flux entering the current sheet with the reconnection inflow.

In this work, we follow the practice of Reeves & Forbes (2005) using $S(t)$ to represent the output power of the radiative energy. Because most of the released magnetic energy is converted into thermal energy in a solar eruption, Reeves (2006) only consider the thermal energy instead of radiative energy. We are able to do so because $S(t)$ is a kind of description for the amount of magnetic energy brought into the current sheet per unit time by the reconnection inflow, and it is eventually dissipated by reconnection and converted into radiative and kinetic energy of the reconnected plasma, as well as the kinetic energy of energetic particles accelerated, in the current sheet. The radiative energy could account for both the thermal and non-thermal components of the emission observed, and the energetic particles may produce non-thermal emission through various ways, such as synchrotron, cyclotron, bremsstrahlung, and so on. Therefore, it is the conversion of this part of magnetic energy that could contribute to the emission accounting for the observed

light curve in the eruption (see also discussions by Reeves & Forbes 2005).

Observationally, the consequences of the energy conversion in the eruption are two-fold. First of all, like its solar counterpart, the current sheet itself is a dense heat source because a reasonably large amount of the magnetic energy is converted into heat there as indicated by observations and models of the solar eruptive cases (e.g., see Reeves et al. 2010; Qiu et al. 2012; Ciaravella et al. 2013; Liu et al. 2013; Susino et al. 2013, and references therein). Since the magnetic field is stronger at low altitudes than at high altitudes, most of the energy released by reconnection mainly occurs in the early stage of the eruption when the ejecta is low and the sheet is short, and the hottest part of the current sheet is then close to the star surface (see e.g. Figure 9 of Reeves et al. 2010). Second, in addition to the direct heating inside the current sheet, a large amount of energetic particles and a heat conduction front are also created by reconnection, and then propagate downward along magnetic field lines (e.g., see Reeves et al. 2007; Winter et al. 2011; Zharkova et al. 2011; Yan et al. 2013, and references therein). They eventually reach the star surface, yielding observational consequences.

The kinetic energy of particles is quickly converted into thermal and non-thermal energy due to collisions of particles with the star surface, and the conduction front dumps all the thermal energy it brings to the surface region leading to the further heating. Therefore, a very hot region, namely the “fireball”, would be naturally expected to form near the star during the giant flare process (see also Figure 4d of Masada et al. 2010). [A schematic description of this scenario can be found in Figure 1 of Lin et al. (2005), which describes the origin of the solar counterpart of the “fireball”, and interested readers are referred to that work.] Thus, the trapped “fireball” as discussed by many authors (e.g., see also Thompson & Duncan 1995; Hurley et al. 2005, for example) is a straightforward and natural consequence of our model, and the emission that comes from this area may account for various observational consequences.

From Faraday's Law, $E_z(t)$ is given by

$$E_z(t) = -\frac{1}{c} \frac{\partial A_0^0}{\partial t} = M_A V_A B_y(0, y_0)/c, \quad (11)$$

where $A_0^0 = A(0, p \leq y \leq q)$ is the magnitude of the vector potential along the current sheet, M_A is the Alfvén Mach number of the reconnection inflow and is a measure of the reconnection rate in the current sheet (Lin & Forbes 2000), is directly proportional to $E_z(t)$, and equals to the reconnection inflow speed compared to the local Alfvén speed near the reconnection region. In this work, it is taken to be a constant at $y_0 = (p + q)/2$, the height of the current sheet center, and the magnetic field B_y is evaluated at y_0 . In the inner magnetosphere of magnetar, the Alfvén velocity $V_A \simeq c$ (Lyutikov 2006).

By calculating the Poynting flux in the current sheet, we can obtain the power related to the energy dissipated in current sheet. Substituting equations (4) and (11) into equation (10) and integrating, we have

$$\begin{aligned} S(t) &= -\frac{c}{2\pi} \left(\frac{2I_0}{c} \right)^2 \frac{M_A \lambda^2 (h^2 + \lambda^2)^2 \sqrt{(y_0^2 - p^2)(q^2 - y_0^2)}}{q(h^2 - y_0^2)(y_0^2 + \lambda^2)(p^2 + \lambda^2)(q^2 + \lambda^2)} \\ &\times \left[\frac{p^2 + \lambda^2}{h^2 + \lambda^2} \Pi \left(\frac{q^2 - p^2}{q^2 + \lambda^2}, \frac{\sqrt{q^2 - p^2}}{q} \right) + \frac{h^2 - p^2}{h^2 + \lambda^2} \Pi \left(\frac{q^2 - p^2}{q^2 - h^2}, \frac{\sqrt{q^2 - p^2}}{q} \right) \right. \\ &\left. - K \left(\frac{\sqrt{q^2 - p^2}}{q} \right) \right], \end{aligned} \quad (12)$$

where K and Π are the complete elliptic integral of the first kind and the third kind, respectively.

According to the law of the universal gravitation, the rate of change in the gravitational potential energy is

$$\frac{dW_{gra}}{dt} = \frac{GM_{NS}\gamma m_0}{(R_0 + h)^2} \dot{h}. \quad (13)$$

Combining equations (8), (9), (10) and (13), we get

$$\frac{dW_{mag}}{dt} = -\frac{B_0^2 \lambda^4}{8hL_{PQ}^2} \left[\frac{H_{PQ}^2}{2h^2} - \frac{(p^2 + \lambda^2)(h^2 - q^2) + (q^2 + \lambda^2)(h^2 - p^2)}{h^2 + \lambda^2} \right] \dot{h} - S(t), \quad (14)$$

which is the expression of Poynting’s theorem for the system studied in the present work (see also Reeves & Forbes 2005; Reeves 2006).

We define the time when the neutral point forms as t_n and $W_{EM}(t_n) = 0$ because no magnetic reconnection occurs at this time, and the magnetic energy at t_n is (Forbes & Priest 1995)

$$W_{mag}(h_n, t_n) = \left(\frac{A_0}{\pi}\right)^2 \left[J_n^2 \ln \left(\frac{2h_n J_n}{r_{00}} \right) + \frac{1}{2} J_n^2 + \frac{1}{4} \right], \quad (15)$$

where J_n and h_n are correspondingly the current and the height of the flux rope at this time, respectively, r_{00} is the radius of the flux rope at the maximum current point.

According to Lin et al. (2004) and Lin & Soon (2004), ejecta brings a large amount of magnetic flux away from the star as well. This flux includes two components: one is associated with the flux rope before the eruption, and another one is brought from the background to the ejecta by magnetic reconnection through the current sheet. So the former is constant during the eruption, and the latter increases after reconnection commences causing the ejecta to expand rapidly. Freezing of the magnetic field to the plasma yields that the magnetic flux and the associated plasma sent to the ejecta by reconnection constitute the outer shell of the ejecta, and the flux is given by

$$\Phi_B = L \left[\frac{I_0 \pi}{c} - A(0, q) \right], \quad (16)$$

where $A(0, q)$ is the value of Equation (5) at the upper tip of the current sheet, which is (Lin & Forbes 2000)

$$A(0, q) = \frac{2I_0}{c} \frac{\lambda}{qL_{PQ}} \left[(h^2 - q^2) K \left(\frac{p}{q} \right) (q^2 - p^2) + \Pi \left(\frac{\lambda^2 + p^2}{\lambda^2 + q^2}, \frac{p}{q} \right) - \frac{H_{PQ}^2}{h^2} \Pi \left(\frac{p^2}{h^2}, \frac{p}{q} \right) \right]. \quad (17)$$

Given p , q , h , and \dot{h} , we can obtain the total magnetic flux brought into interstellar space by magnetic reconnection as a function of time t in the whole process of the eruption.

2.3. Equations Governing Motions Of Ejecta

As the system evolves dynamically and the ejecta moves upward at speed \dot{h} , the electric field E_z in equation (11) can be written as

$$\begin{aligned}
 E_z(t) &= -\frac{1}{c} \frac{\partial A_0^0}{\partial t} = -\frac{1}{c} \frac{\partial A_0^0}{\partial h} \dot{h} \\
 &= -\frac{\dot{h}}{c} \left(\frac{\partial A_0^0}{\partial p} p' + \frac{\partial A_0^0}{\partial q} q' + \frac{\partial A_0^0}{\partial h} \right) \\
 &= -\frac{\dot{h}}{c} (A_{0p} p' + A_{0q} q' + A_{0h}), \tag{18}
 \end{aligned}$$

where $\dot{h} = dh/dt$, $p' = dp/dh$ and $q' = dq/dh$. To find the variations of \dot{h} , p and q versus the flux rope height h , we need two other equations: the frozen-flux condition at the surface of the flux rope and the dynamic equation describing the flux rope acceleration due to the force acting upon it.

For the frozen-flux condition at the surface of the flux rope, we get

$$\frac{2I_0}{c} A_R = A(0, h - r_0) = \text{const}, \tag{19}$$

where r_0 is the radius of the flux rope. Taking the total derivate about h on the both side of the equation (19) gives

$$\frac{\partial A_R}{\partial p} p' + \frac{\partial A_R}{\partial q} q' + \frac{\partial A_R}{\partial h} = A_{Rp} p' + A_{Rq} q' + A_{Rh} = 0. \tag{20}$$

Here p' and q' can be obtained from (18) and (20):

$$p' = \frac{\tilde{A}_{0h} A_{Rq} - A_{Rh} A_{0q}}{A_{Rp} A_{0q} - A_{0p} A_{Rp}}, \tag{21}$$

$$q' = \frac{A_{Rh} A_{0p} - \tilde{A}_{0h} A_{Rp}}{A_{Rp} A_{0q} - A_{0p} A_{Rp}}, \tag{22}$$

where $\tilde{A}_{0h} = cE_z/\dot{h} + A_{0h}$ and the electric field E_z is determined by equation (11).

The dynamic equation is taken from equation (9)

$$\gamma^3 \frac{d^2 h}{dt^2} = \frac{B_0^2 \lambda^4}{8hm_0 L_{PQ}^2} \left[\frac{H_{PQ}^2}{2h^2} - \frac{(p^2 + \lambda^2)(h^2 - q^2) + (q^2 + \lambda^2)(h^2 - p^2)}{h^2 + \lambda^2} \right] - \frac{GM_{NS}\gamma}{(R_0 + h)^2}. \quad (23)$$

Eventually, we obtain equations that govern the motion of the flux rope after the catastrophe:

$$\frac{dh}{dt} = \dot{h}, \quad (24)$$

$$\frac{dp}{dt} = p'\dot{h}, \quad (25)$$

$$\frac{dq}{dt} = q'\dot{h}, \quad (26)$$

$$\begin{aligned} \frac{d^2 h}{dt^2} &= \frac{B_0^2 \lambda^4}{8hm_0 \gamma^3 L_{PQ}^2} \left[\frac{H_{PQ}^2}{2h^2} - \frac{(p^2 + \lambda^2)(h^2 - q^2) + (q^2 + \lambda^2)(h^2 - p^2)}{h^2 + \lambda^2} \right] \\ &- \frac{GM_{NS}}{\gamma^2 (R_0 + h)^2}. \end{aligned} \quad (27)$$

So far, we are ready to investigate the dynamical properties of the system following the catastrophe by solving differential equations (24) through (27). We also further study the energetics of the system via solving equations (10), (13), and (14) consequently by considering equations (12). We note here that equations (21) and (22) should be used when we solve equations (24) through (27).

3. Results

The characteristic values of several important parameters that are specifically for the SGR 1806 - 20 and the associated environment around it can be given according to the observational events we collected so far. These parameters are R_0 , the radius of the neutron star, λ_0 , the half-distance between the two point-sources as the catastrophe occurs (see Figure 2), m , the mass initially included in the flux rope, and L , the length of the flux rope.

We note here that the equations listed previously for governing the emission or light curve of the giant flare and the dynamic properties of the associated mass ejection look very complex

and include many parameters, but only a couple of them are free parameters and the others can be fixed for the specific cases. These parameters include the mass of the neutral star M_{NS} , the initial scale of the eruption L , the magnetic field strength on the star surface B_0 , the mass inside the flux rope m_0 , and the rate of magnetic reconnection M_A . Among them, the value of M_{NS} is fixed, the scale L is taken as the radius of the neutral star that is fixed, the magnetic field B_0 on the surface is also fixed, and only m_0 and M_A leave some room to be adjusted in our calculations in order to obtain theoretical results that are in agreement with observations. Below we shall see that even m_0 could be determined to a certain degree according to observations.

As for M_A , unfortunately, there is not an acceptable value or theory for its value in the case of the eruption on the magnetar for the time being. So we have to resort to the existing results for M_A in the case of solar eruptions. Basically, the standard theory of magnetic reconnection requires that M_A range from 0 to 1 (e.g., see Priest & Forbes 2000; Lin et al. 2003), and observations of solar eruptions put the value of M_A in the range from 0.001 to 0.1 (e.g., see Yokoyama et al. 2001; Lin et al. 2005, 2007). This gives us some flexibility to choose the value of M_A so that our theoretical results would be consistent with observations. We understand that this inevitably brings unexpected uncertainties to our results, and we look forward to more new observations that will help us constrain these free parameters and improve our model further in the future.

Since the energy involved in the magnetar giant flare requires that a large fraction of the magnetosphere be affected, the typical size of an active region is of the order of the neutron star radius (Lyutikov 2006). The distance between the two point-sources, $2\lambda_0$, and the length of the flux rope, $L = 2\lambda_0$, are of the order of the neutron star radius, R_0 ; and we choose $\lambda_0 = R_0/2$ in our calculation because this scale of the magnetic field may provide enough magnetic energy to power a giant flare. The Australia Telescope Compact Array and the Very Large Array observed an expanding radio nebula associated with the giant flare from magnetar SGR 1806-20 (Taylor et al. 2005; Cameron et al. 2005; Gaensler et al. 2005), which implies a large scale

mass ejection in the eruptive process that produced the giant flare. Similar explosive phenomenon of the giant flare together with a mass ejection may also occur in a black hole accretion disk system, which is also known as an episodic jet (e.g., see also Yuan et al. 2009). If the ejecta is roughly spherical, the radiation is well-explained by synchrotron emission from a shocked baryonic shell with a mass of $\geq 10^{24.5}$ g and an expansion velocity of $\simeq 0.4c$ (Gaensler et al. 2005; Granot et al. 2006; Masada et al. 2010). We choose $m = 10^{26}$ g because the ejecta can be ejected outward successfully at a reasonable velocity. If the mass is too heavy, it may not be thrown away successfully; on the other hand, if the ejecta is too light, it will travel too fast to fit the observational result. According to these facts, we choose the characteristic values of these parameters mentioned above as below:

$$R_0 = 10^6 \text{ cm}, \lambda_0 = 5 \times 10^5 \text{ cm}, m = 10^{26} \text{ g}.$$

Solving equation (24) through (27) with $M_A = 0.02$ (according to our experience in dealing with the solar case) gives the time profiles of the flux rope height h , the lower top and the upper top, p and q , of the current sheet, respectively. The results are plotted in Figure 4, and the corresponding velocity of the flux rope is plotted in Figure 5, which indicates that the flux rope is thrust away from the star surface very quickly and can be easily accelerated to a speed of $0.5c$ within several milliseconds following the catastrophe. This time interval roughly fits that of the impulsive phase of the eruption from SGR 1806-20. We shall further discuss the issue related to the time scale of the eruption later. The released magnetic energy is enough to be converted into kinetic energy that could accelerate the flux rope to high speed. The flux rope is thrust outward by the catastrophe rapidly at the beginning stage of the eruption, and the reconnection process invoked in the current sheet following the catastrophe allows the flux rope to propagate continuously at high speed for a while (see discussions of Lin & Forbes 2000; Lin 2002). Therefore, the flux rope or the ejecta could go very far away from the central star after the eruption commences.

Then we get the variations of the total magnetic flux sent into interstellar space by reconnection versus time for magnetar SGR 1806- 20 giant flare for $B = 10^{15}$ G in Figure 6. The preexisting magnetic flux inside the flux rope prior to the eruption was $\Phi_p = I_0\pi/cL \approx 7.85 \times 10^{26}$ Mx (see also Lin et al. 2004; Lin & Soon 2004), and the total magnetic flux brought into space by reconnection in the whole process is about 6.7×10^{26} Mx, where Mx = 10^{-8} Wb is the CGS unit of the magnetic flux . Therefore, the eruption brought more than 1.5×10^{27} Mx of magnetic flux away from the central star. Time histories of the total magnetic flux of SGR 1900+14 and SGR 0526-66 related to reconnection are also shown in Figure 6 for $B = 5.0 \times 10^{14}$ G for both events, and the total magnetic fluxes sent into interstellar space during the eruption were 6.9×10^{26} Mx for SGR 1900+14 and 6.7×10^{26} Mx for SGR 0526-66, respectively.

The energy budget for the eruption in our model is calculated and shown in Figure 7. The total energy involved in the eruption W_0 consists of free magnetic energy, kinetic energy, gravitational potential energy and radiative energy (see also equation (7)). If we take the gravitational potential energy to be zero right before the catastrophe, W_0 is identified with W_{mag} as the catastrophe is invoked. In the process of eruption W_{mag} keeps decreasing and the other types of energy as the left side of equation (7) continuously increase.

Our calculations indicate that the free magnetic energy stored in the system prior to the eruption is more than 10^{47} erg which seems to be enough to power the giant flare from magnetar SGR 1806 - 20 on 27 December 2004. But we need to check whether all of this stored magnetic energy or just part of it could be quickly converted into radiation and accelerating plasma to account for the giant flare and the associated mass ejection. Usually, the eruption starts with the catastrophe and reconnection helps the eruption develop smoothly (Lin & Forbes 2000; Lin 2002). So the rate of the energy release is governed by both the catastrophe and the following reconnection process. Generally, the energy release rate reaches maximum in the catastrophic

stage. But two facts prevent most of the energy release from taking place in the catastrophic stage: first, the time scale of the catastrophe is too short (several hundred seconds for a solar eruptive event and several tenth ms for the magnetar case) to allow the main energy release to occur; and second, the ideal MHD nature of the catastrophe leads to the development of a current sheet that halts the further evolution after a very short period in the initial stage unless the ideal MHD environment breaks down (e.g., see Forbes & Isenberg 1991; Isenberg et al. 1993).

Compared to the catastrophe, the reconnection has long time scale (a few 10^3 seconds in the solar case, and a few ms in the magnetar case), so the energy conversion could be taking place gradually and lasting long. Additionally, reconnection is a totally non-ideal MHD process, and the magnetic field can be quickly diffused with its energy being converted into other types of energy during this process, thus allowing the eruptive process to develop smoothly.

Therefore, in an eruptive process, no matter whether on the Sun or on a magnetar, most of the free energy is converted into radiative and kinetic energies via magnetic reconnection (see detailed discussions on this issue by Forbes et al. 1994; Forbes & Priest 1995), and the time scale of the magnetic reconnection determines the subsequent evolution in the system. Figure 7 plots time profiles of various types of energy for SGR 1806-20, from which we see that after a transient stage of a few tenth ms (see also Figure 5), the evolution in the system turns to a gradual phase within several ms, and the main energy conversion happens within this several ms.

In addition, we also noticed that the energy conversion lasts for a very long period at a very low rate (but not zero) after the progress discussed above, and that not all the free energy is released in the whole process although W_{mag} drops apparently from its initial value to a low value. The difference between the initial value of W_{mag} and that of W_{mag} at least 500 seconds after is more than 1×10^{47} erg, which is enough to produce a giant flare and the associated mass ejection that have ever been observed by several instruments.

After the catastrophe takes place, the flux rope is quickly ejected away from the star's surface,

a small fraction of released magnetic energy is partly converted into kinetic energy and is partly used to do the work against the gravity in the catastrophe (see also Figure 3). Formation of the X-point is followed by the development of the current sheet, which is expected to be long because the reconnection process is slow compared to the catastrophe. The existence of the X-point and / or the current sheet allows reconnection to occur, and the magnetic energy is converted into radiative and kinetic energy. In this process, the magnetic field at either side of current sheet, which is responsible for the magnetic tension that prevents the flux rope from moving far, approaches the shear giving rise to the Poynting flux into the sheet. Magnetic reconnection dissipates this magnetic field, weakening the magnetic tension, heating the plasma, and allowing the flux rope to escape from the center star (see also discussions in detail by Forbes & Lin 2000; Lin & Forbes 2000; Lin 2002).

As shown in Figure 7, W_{mag} quickly decreases in the early stage, and the kinetic and gravitational potential energy of the flux rope, together with the Poynting flux and the associated emission, increases rapidly. This process occurs within the first millisecond in a very energetic fashion. When the flux rope achieves escape velocity, the energy released approaches an asymptotic value at long times. It is simple and straightforward to prove that the amount of decrease in W_{mag} is just equal to the sum of increases in W_{ke} , W_{gra} and W_{EM} .

The power output associated with radiative energy is directly related to $S(t)$ as indicated by equation (10) and the related discussions right after the equation. So the time profile of $S(t)$ could be considered the light curve of the event. Figure 8 gives $S(t)$ as a function of t . It shows that after the neutral point forms, the energy output rate curve has a hard spike in the first several milliseconds, and then turns to a tail emission lasting hundreds seconds. The shape of the light curve given by our model is very reminiscent of the light curve of the giant flare from magnetar SGR 1806- 20 on 27 December 2004. To compare our results with those of the giant flare from magnetar SGR 1806- 20 on 27 December 2004 observed by RHESSI γ - ray detectors, we create a

composite of the modified light curve from Figure 8 and the observed one (see Figure 9).

As shown in Figure 9, the black curve is from the giant flare 20-100-keV time history plotted with 0.5-s resolution, and red curve is from our model. The time $t = 0$ corresponds to 77,400 s UT. In this plot, the flare began with the spike at 26.64 s and saturated the detectors within 1 ms. The detectors emerged from saturation on the falling edge 200 ms later and remained unsaturated after that. Photons with energies ≥ 20 keV are unattenuated; thus the amplitude variations in the oscillatory phase are real, and are not caused by any known instrumental effect (Hurley et al. 2005). We noticed in Figure 9 that the observed data consist of 3 phases: a 1-s long precursor, an initial spike of the giant flare which lasts for 0.2 s and an oscillatory tail modulated with a period of 7.56 s.

On the basis of our model and with assumptions that the energy was composed of photons with an average energy of 60 keV and that the detected energy is proportional to $\sim 4\pi d^2 S(t)$, where $d \approx 15$ kpc is the distance between the Earth and the SGR 1806-20 (Corbel & Eikenberry 2004; Cameron et al. 2005; McClure-Griffiths & Gaensler 2005), we obtain the light curve of the giant flare for the case where the outburst is spherical for simplicity. The time when the X-point appears corresponds to 77,426.6 s UT on 27 December 2004 in our calculations. In Figure 9, We see a good agreement of our model with observations. In this work, we do not include the precursor of the giant flare because our calculations start at the moment when the system loses its equilibrium. The precursor may be explained by the plastic deformation of the crust (Lyutikov 2006), crust motions (Ruderman 1991a), or other mini scale eruptions like what happens frequently in the solar eruptions (e.g., see Jiang et al. 2011; Shen et al. 2012).

Using the same methods, we are also able to calculate the light curves of the giant flares from SGR 0526-66 and SGR 1900+14, and compare them with the observations as shown in Figures 10 and 11, respectively. The observational data for SGR 0526-66 were detected by Venera 11 (Mazets et al. 1979), and the energy range covered 50-150 keV, the time cadence of the

observation was $1/4$ s, and the burst onset time t_0 for Venera 11 was 15 h 51 min 39 s, 145 UT. The distance used in our calculation was $d = 55$ kpc (Mazets et al. 1979) for this event.

The observations for the 27 August 1998 event were performed by Ulysses from the 0.5-s resolution continuously available real-time data (Hurley et al. 1999), which had 25-150 keV time history and were corrected for dead-time effects. Zero seconds corresponds to 37,283.12s UT at the Earth, and $d = 7$ kpc (Hurley et al. 1999) for SGR 1900+14. As shown in Figures 10 and 11, our results fit the observational ones well.

4. Discussions and Conclusions

We develop a theoretical model via an analytic approach for a magnetar giant flare in the framework of the solar CME catastrophe model (Lin & Forbes 2000). We considered the physical process that causes the catastrophic loss of equilibrium of a twisted flux rope in the magnetar magnetosphere. The model was constructed according to manifestations of the eruption from the magnetar SGR 1806-20. As happens on the Sun, the free magnetic energy that drives the eruption on the magnetar is slowly stored in the magnetosphere of the magnetar long before the outburst until the system loses mechanical equilibrium, and then is quickly released in the consequent eruptive process, also known as a magnetar giant flare. In our model, the energy driving the eruption comes from the magnetosphere. The motion of footpoints causes the magnetic configuration to lose its equilibrium and release magnetic energy eventually, which is in principle the same as the results of numerical simulations (Parfrey et al. 2012a,b, 2013; Yu 2011, 2012).

In the present model, the eruption starts with a loss of equilibrium in the magnetic configuration, which could be triggered either by the change in the background magnetic field, or by the sudden break of a crust piece on the surface of the star where the disrupting magnetic configuration roots in. The evolution in this stage could be purely mechanical, namely

no dissipation or magnetic reconnection needs to take place in the magnetosphere. But the dissipation is required in the consequent progress, otherwise the conversion of magnetic energy into radiative and kinetic energy would be stopped, and the evolution in the system ceases without plausible eruptive phenomenon happening (e.g., see detailed discussions by Forbes & Lin 2000; Lin & Forbes 2000; Lin 2002; Priest & Forbes 2002; Lin et al. 2003; Forbes et al. 2006).

Our main results deduced from the present analysis are summarized as follow:

1. The system could store free energy of more than 10^{47} ergs prior to the eruption, which is enough to drive a giant flare like the one from magnetar SGR 1806-20 observed on 27 December 2004.

2. A combination of the following three factors determines that the disrupting magnetic configuration is highly stretched, and a long magnetically neutral current sheet forms separating two magnetic fields of opposite polarity. These factors are the mechanical property of the loss of equilibrium, the inertia of the magnetic field that tends to keep the original topological features in the configuration unchanged without diffusion in the system (see detailed discussions by Forbes & Isenberg 1991; Isenberg et al. 1993), and the fact that the reconnection time-scale is long compared to that of the loss of equilibrium.

3. A long current sheet is usually unstable to perturbations due to various plasma instabilities, such as the tearing mode instability, and the consequent turbulence quickly dissipates the magnetic field such that the stored magnetic energy is rapidly converted into radiative and kinetic energy of the plasma inside the current sheet, as well as the kinetic energy and the gravitational potential energy of the mass in the ejected flux rope. Most of the released magnetic energy turns into radiative energy in the case of the giant flare from SRG 1806-20.

4. Conversion of energy by reconnection mainly occurs at the lower part of the current sheet, and the hottest part of the current sheet is then expected close to the star surface. A large amount

of energetic particles and a heat conduction front are also created by reconnection and propagate downward along magnetic field lines. They eventually reach the star surface and may heat the relevant region significantly, which then leads to the formation of a “fireball” near the neutron star’s surface. Therefore, a “fireball” is a straightforward and natural consequence of our model.

5. We calculated the light curve on the basis of our model and compare it with the observational one obtained by the RHESSI γ -ray detectors. We note that the calculated light curve consists of a hard spike lasting a half ms and a tail emission last a few 10^2 s, which are consistent with the observations.

6. Our calculations indicate that the magnetic flux preexisting in the flux rope before the eruption was about 7.9×10^{26} Mx, and that the magnetic flux brought from the environment around the disrupting magnetic field into the ejecta bubble was around 6.8×10^{26} Mx. Therefore, total magnetic flux of more than 1.5×10^{27} Mx was sent into interstellar space from the central star by the super eruption from SGR 1806-20.

7. We duplicated our calculations for the giant flares from SGR 0526-66 and SGR 1900+14, respectively, and also found good agreement of our model with observations. Furthermore, the the total magnetic fluxes ejected into interstellar space by the eruption were 6.9×10^{26} Mx for SGR 1900+14 and 6.7×10^{26} Mx for SGR 0526-66, respectively.

We are grateful to K. Hurley for providing the observational data used in this paper, and to Z. Dai and Y. Yuan for valuable discussions and suggestions. Helpful advice and suggestions for using the observational data given by D. M. Palmer are highly appreciated. We appreciate the referee for constructive advice and comments for improving this work as well. This work was supported by Program 973 grants 2011CB811403 and 2013CBA01503, NSFC grants 11273055 and 11333007, and CAS grants KJCX2-EW-T07 and XDB09000000. F. Y. was supported by the NSFC grants 11121062 and 11133005. K. K. R. is supported by NSF grant AGS-1156076 to the

Smithsonian Astrophysical Observatory.

A. Appendix

The motion of flux rope is described by four parameters (h, p, q, \dot{h}) , which are the height of flux rope, heights of the lower and higher tips of the current sheet, and the velocity of flux rope, respectively. Another three independent equations are required in solving Equation (1). In this section, the required equations are simply described. They are based on Lin & Forbes (2000), Lin et al. (2006) and Yuan et al. (2009).

The forces acting on the flux rope include the magnetic force, F_m (the first term on the right hand side of equation (1), and the gravity, F_g (the second term), which read as

$$F_m = \frac{B_0^2 \lambda^4}{8hL_{PQ}^2} \left[\frac{H_{PQ}^2}{2h^2} - \frac{(p^2 + \lambda^2)(h^2 - q^2) + (q^2 + \lambda^2)(h^2 - p^2)}{h^2 + \lambda^2} \right], \quad (\text{A1})$$

$$F_g = \frac{GM_{NS}\gamma m_0}{(R_0 + h)^2}, \quad (\text{A2})$$

respectively, where $L_{PQ}^2 = (\lambda^2 + p^2)(\lambda^2 + q^2)$, $H_{PQ}^2 = (h^2 - p^2)(h^2 - q^2)$, B_0 and λ are the surface magnetic field strength and the half distance between the two point sources on the surface of the star prior to the eruption, respectively (see also Figure 2). On the right-hand side of equation (A1), the two terms in the square brackets denote the magnetic compression force and the magnetic tension. The magnetic compression force pushes the flux rope upwards and the magnetic tension pulls the flux rope downwards. The system is in equilibrium as they balance each other. When the system loses its equilibrium, the compression dominates the tension, thrusting the flux rope outward in a catastrophic way.

The force-free condition outside the current sheet and the frozen flux condition on the surface of the flux rope can be used to deduce the equations governing the evolution of the current sheet,

which are (Forbes & Isenberg 1991; Lin & Forbes 2000)

$$\begin{aligned}\frac{dp}{dt} &= p'\dot{h}, \\ \frac{dq}{dt} &= q'\dot{h},\end{aligned}\tag{A3}$$

where p' and q' are given in equations (21) and (22) with

$$\tilde{A}_{0h} = \frac{cE_z}{\dot{h}} + A_{0h} = \frac{M_A B_y(0, y_0)c}{\dot{h}} + A_{0h},\tag{A4}$$

where $B_y(0, y_0)$ can be deduced from equation (4), and

$$\begin{aligned}A_R &= \frac{\lambda H_{PQ}}{2h L_{PQ}} \ln \left[\frac{\lambda H_{PQ}^3}{r_{00} L_{PQ} (h^4 - p^2 q^2)} \right] \\ &+ \tan^{-1} \left(\frac{\lambda}{h} \sqrt{\frac{p^2 + \lambda^2}{q^2 + \lambda^2}} \sqrt{\frac{h^2 - q^2}{h^2 - p^2}} \right) + \frac{\lambda}{q L_{PQ}} \left\{ (h^2 - q^2) F \left[\sin^{-1} \left(\frac{q}{h} \right), \frac{p}{q} \right] \right. \\ &+ (q^2 - p^2) \Pi \left[\sin^{-1} \left(\frac{q}{h} \right), \frac{p^2 + \lambda^2}{q^2 + \lambda^2}, \frac{p}{q} \right] - \frac{H_{PQ}^2}{h^2} \Pi \left[\sin^{-1} \left(\frac{q}{h} \right), \frac{p^2}{h^2}, \frac{p}{q} \right] \left. \right\} \\ &= \frac{\pi}{4} + \ln \left(\frac{2\lambda}{r_{00}} \right), \\ A_{Rp} &= \frac{\lambda p (h^2 + \lambda^2)}{q (p^2 + \lambda^2)^2} \sqrt{\frac{p^2 + \lambda^2}{q^2 + \lambda^2}} \left\langle \left(1 - \frac{p^2}{h^2} \right) \Pi \left[\sin^{-1} \left(\frac{q}{h} \right), \frac{p^2}{h^2}, \frac{p}{q} \right] \right. \\ &- F \left[\sin^{-1} \left(\frac{q}{h} \right), \frac{p}{q} \right] - \frac{q}{2h} \sqrt{\frac{h^2 - q^2}{h^2 - p^2}} \left\{ 1 + \ln \left[\frac{\lambda H_{PQ}^3}{r_{00} L_{PQ} (h^4 - p^2 q^2)} \right] \right\} \left. \right\rangle, \\ A_{Rq} &= \frac{\lambda (h^2 + \lambda^2)}{(q^2 + \lambda^2)^2} \sqrt{\frac{q^2 + \lambda^2}{p^2 + \lambda^2}} \left\langle \left(1 - \frac{p^2}{h^2} \right) \Pi \left[\sin^{-1} \left(\frac{q}{h} \right), \frac{p^2}{h^2}, \frac{p}{q} \right] \right. \\ &- F \left[\sin^{-1} \left(\frac{q}{h} \right), \frac{p}{q} \right] - \frac{q}{2h} \sqrt{\frac{h^2 - p^2}{h^2 - q^2}} \left\{ 1 + \ln \left[\frac{\lambda H_{PQ}^3}{r_{00} L_{PQ} (h^4 - p^2 q^2)} \right] \right\} \left. \right\rangle, \\ A_{Rh} &= \frac{\lambda}{2h^2 L_{PQ} H_{PQ}} \left\{ 2 \frac{h^6 - \lambda^2 p^2 q^2}{h^2 + \lambda^2} - \frac{h^2 (p^2 + q^2) (h^2 - \lambda^2)}{h^2 + \lambda^2} \right. \\ &+ (h^4 - p^2 q^2) \ln \left[\frac{\lambda H_{PQ}^3}{r_{00} L_{PQ} (h^4 - p^2 q^2)} \right] \left. \right\} + \frac{\lambda}{hq L_{PQ}} \\ &\times \left\{ (h^2 + q^2) F \left[\sin^{-1} \left(\frac{q}{h} \right), \frac{p}{q} \right] - q^2 E \left[\sin^{-1} \left(\frac{q}{h} \right), \frac{p}{q} \right] \right. \\ &- \left. \frac{h^4 - p^2 q^2}{h^2} \Pi \left[\sin^{-1} \left(\frac{q}{h} \right), \frac{p^2}{h^2}, \frac{p}{q} \right] \right\}.\end{aligned}\tag{A5}$$

and

$$\begin{aligned}
A_0^0 &= \frac{2I_0}{c} \frac{\lambda}{qL_{PQ}} \left[(h^2 - q^2)K\left(\frac{p}{q}\right) + (q^2 - p^2) \right. \\
&\quad \times \left. \Pi\left(\frac{p^2 + \lambda^2}{q^2 + \lambda^2}, \frac{p}{q}\right) - \frac{H_{PQ}^2}{h^2} \Pi\left(\frac{p^2}{h^2}, \frac{p}{q}\right) \right], \\
A_{0p} &= \frac{\lambda p (h^2 + \lambda^2) (q^2 + \lambda^2)}{h^2 q [(p^2 + \lambda^2) (q^2 + \lambda^2)]^{3/2}} \\
&\quad \times \left[(h^2 - q^2) \Pi\left(\frac{p^2}{h^2}, \frac{p}{q}\right) - h^2 K\left(\frac{p}{q}\right) \right], \\
A_{0q} &= \frac{\lambda (h^2 + \lambda^2) (p^2 + \lambda^2)}{h^2 [(p^2 + \lambda^2) (q^2 + \lambda^2)]^{3/2}} \\
&\quad \times \left[(h^2 - q^2) \Pi\left(\frac{p^2}{h^2}, \frac{p}{q}\right) - h^2 K\left(\frac{p}{q}\right) \right], \\
A_{0h} &= -\frac{\lambda}{h^3 q \sqrt{(p^2 + \lambda^2) (q^2 + \lambda^2)}} \\
&\quad \times \left[h^2 q^2 E\left(\frac{p}{q}\right) - h^2 (h^2 + q^2) K\left(\frac{p}{q}\right) \right. \\
&\quad \left. + (h^4 - p^2 q^2) \Pi\left(\frac{p^2}{h^2}, \frac{p}{q}\right) \right], \tag{A6}
\end{aligned}$$

where the specification of K and Π can be found in section 2.2; F and E are first and second kinds of incomplete elliptic integrals, respectively.

REFERENCES

Aly, J. J. 1984, ApJ, 283, 349

Aly, J. J. 1991, ApJ, 375, L61

Cameron, P. B., Chandra, P., Ray, A., Kulkarni, S. R., Frail, D. A., Wieringa, M. H., Nakar, E.,
Phinney, E. S., et al. 2005, Nature, 434, 1112

Ciaravella, A., Webb, D. F., Giordano, S., Raymond, J. C. 2013, ApJ, 766, 65

Corbel, S., & Eikenberry, S. S. 2004, A&A, 419, 191

Duncan, R. C., & Thompson, C. 1992, ApJ, 392, L9

Forbes, T. G., & Isenberg, P. A. 1991, ApJ, 373, 294

Forbes, T. G. 2000, J. Geophys. Res., 105, 23153

Forbes, T. G. 2003, Adv. Space Res., 32, 1043

Forbes, T. G., & Lin, J. 2000, J. Atmos. Sol. Terr. Phys., 62, 1499

Forbes, T. G., & Priest, E. R. 1995, ApJ, 446, 377

Forbes, T. G., Priest, E. R., & Isenberg, P. A. 1994, Sol. Phys., 150, 245

Forbes, T. G.; Linker, J. A., Chen, J., Cid, C., Kóta, J., Lee, M. A., Mann, G., Mikić, Z., et al.
2006, Space Sci. Rev., 123, 251

Gaensler, B. M., Kouveliotou, C., Gelfand, J. D., Taylor, G. B., Eichler, D., Wijers, R. A. M. J.,
Granot, J., Ramirez-Ruiz, E., et al. 2005, Nature, 434, 1104

Gill, R., & Heyl, J. S. 2010, MNRAS, 407, 1926

Götz, D., Mereghetti, S., & Hurley, K. 2007, ApSS, 308, 51

- Granot, J., Ramirez-Ruiz, E., Taylor, G. B., Eichler, D., Lyubarsky, Y. E., Wijers, R. A. M. J., Gaensler, B. M., Gelfand, J. D., et al. 2006, *ApJ*, 638, 391
- Harding, A. K., & Lai, D. 2006, *Rep. Prog. Phys.*, 69, 2631
- Hurley, K., Cline, T., Mazets, E., Barthelmy, S., Butterworth, P., Marshall, F., Palmer, D., Aptekar, R., et al. 1999, *Nature*, 397, 41
- Hurley, K., Boggs, S. E., Smith, D. M., Duncan, R. C., Lin, R., Zoglauer, A., Krucker, S., Hurford, G., et al. 2005, *Nature*, 434, 1098
- Isenberg, P. A., Forbes, T. G., & Démoulin, P. 1993, *ApJ*, 417, 368
- Isenberg, P. A., & Forbes, T. G. 2007, *ApJ*, 670, 1453
- Jiang, Y., Yang, J., Hong, J., Bi, Y., & Zheng, R. 2011, *ApJ*, 738, 179
- Klimchuk, J. A. 2001, in *Space Weather*, ed. P. Song, H. J. Singer & G. Siscoe (Washington, DC: AGU), 143
- Kouveliotou, C., Dieters, S., Strohmayer, T., van Paradijs, J., Fishman, G. J., Meegan, C. A., Hurley, K., Kommers, J., et al. 1998, *Nature*, 393, 235
- Kouveliotou, C., Strohmayer, T., Hurley, K., van Paradijs, J., Finger, M. H., Dieters, S., Woods, P., Thompson, C., 1999, *ApJ*, 510, L115
- Lin, J., & Forbes, T. G. 2000, *J. Geophys. Res.*, 105, 2375
- Lin, J. 2002, *ChJAA*, 2, 539
- Lin, J., Forbes, T. G., & Démoulin, P. 1998, *ApJ*, 504, 1006
- Lin, J., Ko, Y.-K., Sui, L., Raymond, J. C., Stenborg, G. A., Jiang, Y., Zhao, S., Mancuso, S. 2005, *ApJ*, 622, 1251

- Lin, J., Mancuso, S., & Vourlidas, A. 2006, *ApJ*, 649, 1110
- Lin, J., Li, J., Forbes, T. G., Ko, Y.-K., Raymond, J. C., Vourlidas, A. 2007, *ApJ*, 658, L123
- Lin, J., & Soon, W. 2004, *NewA*, 9, 611
- Lin, J., van Ballegooijen, A. A., & Forbes, T. G. 2002, *J. Geophys. Res.*, 107, 1438
- Lin, J., Soon, W., & Baliunas, S. L. 2003, *NewA Rev.*, 47, 53
- Lin, J., Raymond, J. C., & van Ballegooijen, A. A. 2004, *ApJ*, 602, 422
- Liu, W. -J., Qiu, J., Longcope, D. W., Caspi, A. 2013, *ApJ*, 770, 111
- Lyutikov, M. 2003, *MNRAS*, 346, 540
- Lyutikov, M. 2006, *MNRAS*, 367, 1594
- Masada, Y., Nagataki S., Shibata, K., & Terasawa, T. 2010, *PASJ*, 62, 1093
- Mazets, E. P., Golentskii, S. V., Ilinskii, V. N., Aptekar, R. L., Guryan, Iu. A. 1979, *Nature*, 282, 587
- McClure-Griffiths, N. M., & Gaensler, B. M. 2005, *ApJ*, 630, L161
- Mereghetti, S., Tiengo, A., Stella, L., Israel, G. L., Rea, N., Zane, S., & Oosterbroek, T. 2004, *ApJ*, 608, 427
- Palmer, D. M., Barthelmy, S., Gehrels, N., Kippen, R. M., Cayton, T., Kouveliotou, C., Eichler, D., Wijers, R. A. M. J., Woods, P. M., et al. 2005, *Nature*, 434, 1107
- Parfrey, K., Beloborodov, A. M., & Hui, L. 2012a, *MNRAS*, 423, 1416
- Parfrey, K., Beloborodov, A. M., & Hui, L. 2012b, *ApJ*, 754, L12
- Parfrey, K., Beloborodov, A. M., & Hui, L. 2013, *ApJ*, 774, 92

- Parker, E. N. 1963, in *The Physics of Solar Flares*, ed. W. N. Hess (Washington, D. C.: NASA) 425
- Parker, H. E. 1964, *ApJS*, 8, 177
- Priest, E. R., 1982, *Solar Magnetohydrodynamics* (Boston: Reidel)
- Priest, E. R., & Forbes, T. G. 2000, *Magnetic Reconnection: MHD Theory and Applications* (New York: Cambridge Univ. Press)
- Priest, E. R., & Forbes, T. G. 2002, *A & ARv*, 10, 313
- Qiu, J., Liu, W. -J., Longcope, D. W. 2012, *ApJ*, 752, 124
- Reeves, K. K., & Forbes, T. G. 2005, *ApJ*, 630, 1133
- Reeves, K. K. 2006, Ph.D. thesis, Univ. New Hampshire
- Reeves, K. K., Warren, H. P., & Forbes, T. G. 2007, *ApJ*, 668, 1210
- Reeves, K. K., Linker, J. A., Mikic, Z., & Forbes, T. G. 2010, *ApJ*, 721, 1547
- Ruderman, M. 1991a, *ApJ*, 366, 261
- Ruderman, M. 1991b, *ApJ*, 382, 576
- Ruderman, M. 1991c, *ApJ*, 382, 587
- Shen, Y., Liu, Y. & Su, J. 2012, *ApJ*, 750, 12
- Shibata, K., & Yokoyama, T. 1999, *ApJ*, 526, L49
- Sturrock, P. A. 1991, *ApJ*, 380, 655
- Susino, R., Bemporad, A., Krucker, S. 2013, *ApJ*, 777, 93

- Švestka, Z. 1976, *Solar Flares: Geophys. Astrophys. Monogr.* (Dordrecht: Reidel)
- Taylor, G. B., Gelfand, J. D., Gaensler, B. M., Granot, J., Kouveliotou, C., Fender, R. P., Ramirez-Ruiz, E., Eichler, D., et al. 2005, *ApJ*, 634, L93
- Thompson, C., & Duncan, R. C. 1995, *MNRAS*, 275, 255
- Thompson, C., & Duncan, R. C. 1996, *ApJ*, 473, 322
- Thompson, C., & Duncan, R. C. 2001, *ApJ*, 561, 980
- Thompson, C., Lyutikov, M., & Kulkarni, S. R. 2002, *ApJ*, 574, 332
- Thompson, C., & Murray, N. W. 2001, *ApJ*, 560, 339
- Vrba, F., Henden, A. A., Luginbuhl, C. B., Guetter, H. H., Hartmann, D. H., Klose, S. 2000, *ApJ*, 533, L17
- Winter, H. D., Martens, P., & Reeves, K. K. 2011, *ApJ*, 735, 103
- Yan, L., Winter, H. D., Murphy, N. A., Jun, L., Ning, W. 2013, *PASJ*, 65, 101
- Yokoyama, T., Akita, K., Morimoto, T., Inoue, K., Newmark, J. 2001, *ApJ*, 546, L69
- Yu, C. 2011, *ApJ*, 738, 75
- Yu, C. 2012, *ApJ*, 757, 67
- Yuan, F., Lin, J., Wu, K., & Ho, L. C. 2009, *MNRAS*, 395, 2183
- Zharkova, V. V., Arzner, K., Benz, A. O., Browning, P., Dauphin, C., Emslie, A. G., Fletcher, L., Kontar, E. P., et al. 2011, *Space Sci. Rev.*, 159, 357

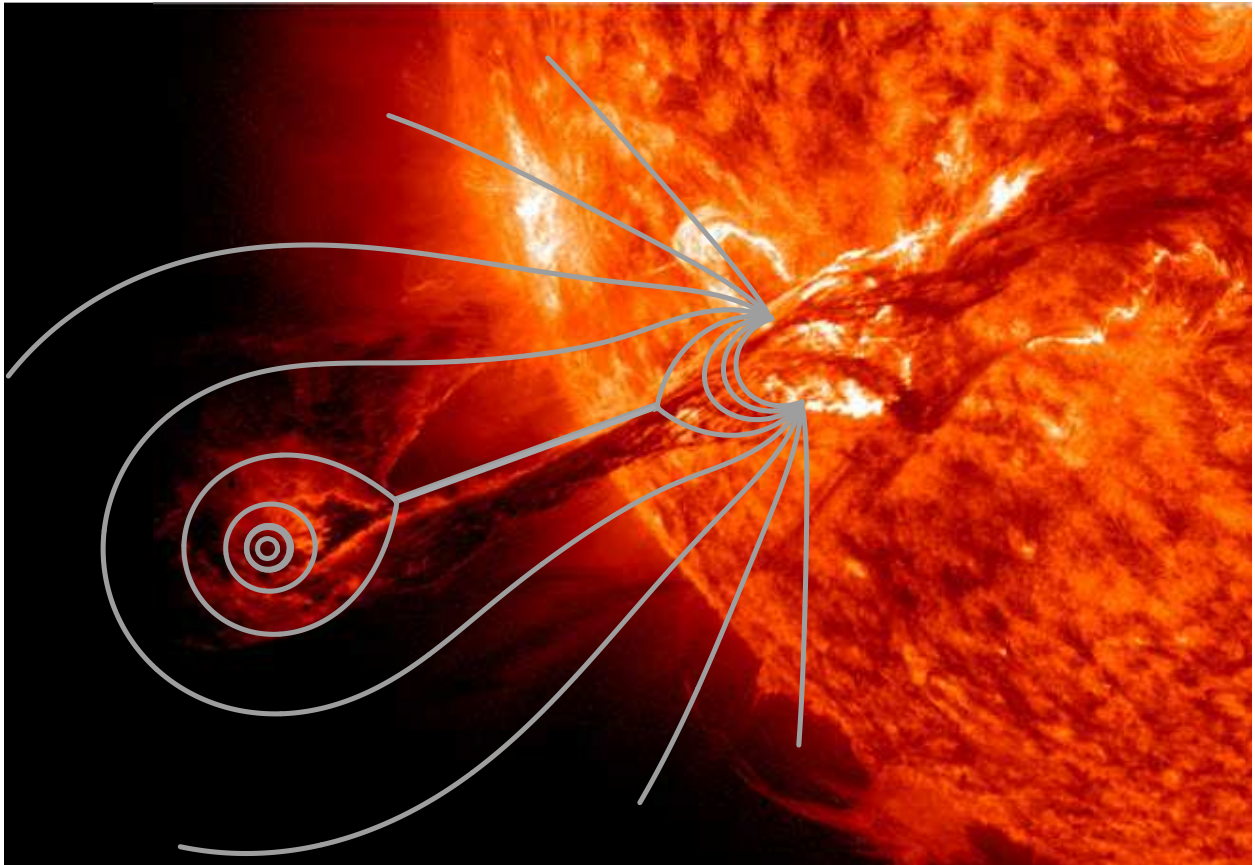


Fig. 1.— Example of a typical eruptive event (namely a CME) occurring in the solar atmosphere (the original image was taken from the SDO website: <http://sdo.gsfc.nasa.gov/>), overlapped with a sketch for describing the surrounding magnetic field in a plane perpendicular to the main axis of the ejecta.

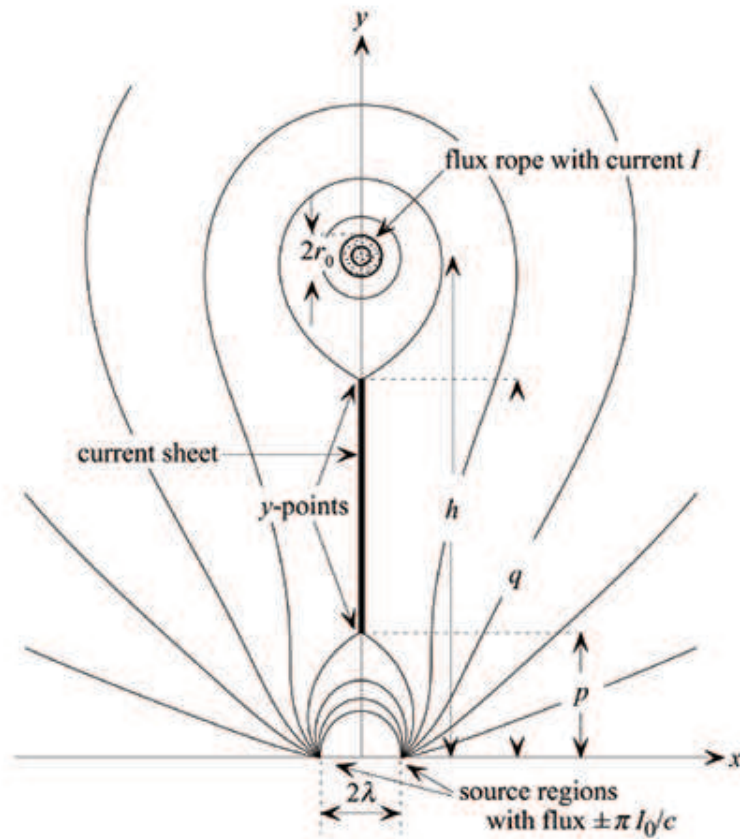


Fig. 2.— Diagram of the flux rope configuration, showing the mathematical notation used in the text from (Lin & Forbes 2000). The x -axis is located on the star surface, and the y -axis points upward. The height of the center of the flux rope is denoted by h , p , and q denote the lower and upper tips of the current sheet, respectively, and the distance between the magnetic source regions on the photosphere is 2λ .

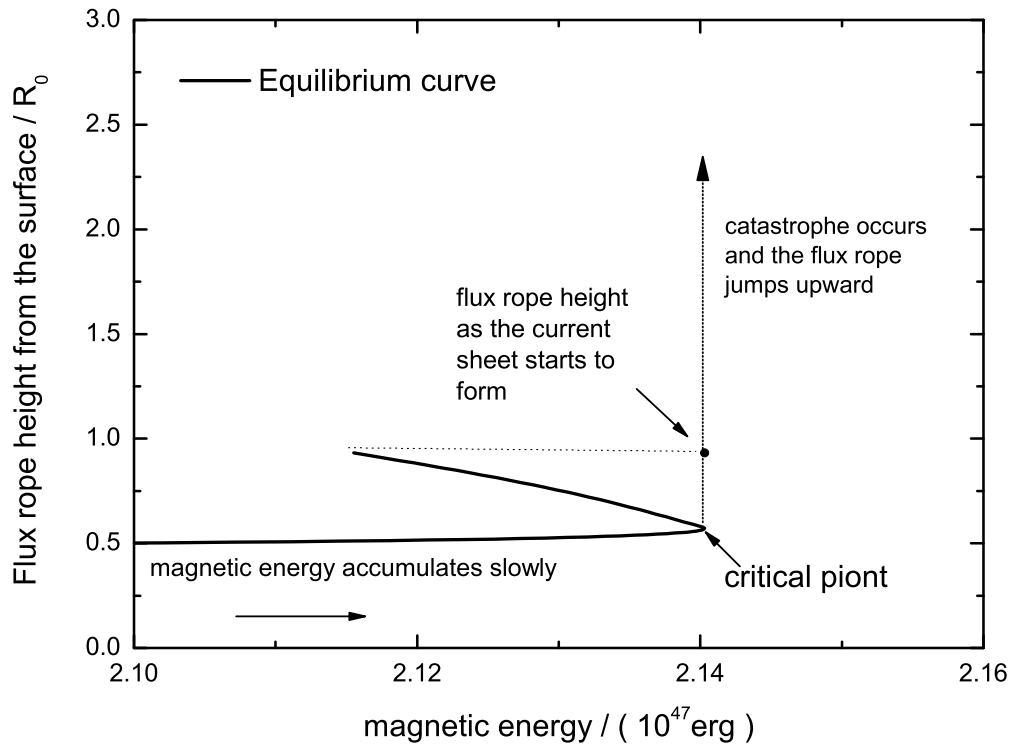


Fig. 3.— Equilibrium flux rope height (in units of the neutron star radius $R_0 \approx 10^6$ cm) as a function of stored magnetic energy. When the critical point is reached, the catastrophe occurs, and the flux rope is ejected outwards.

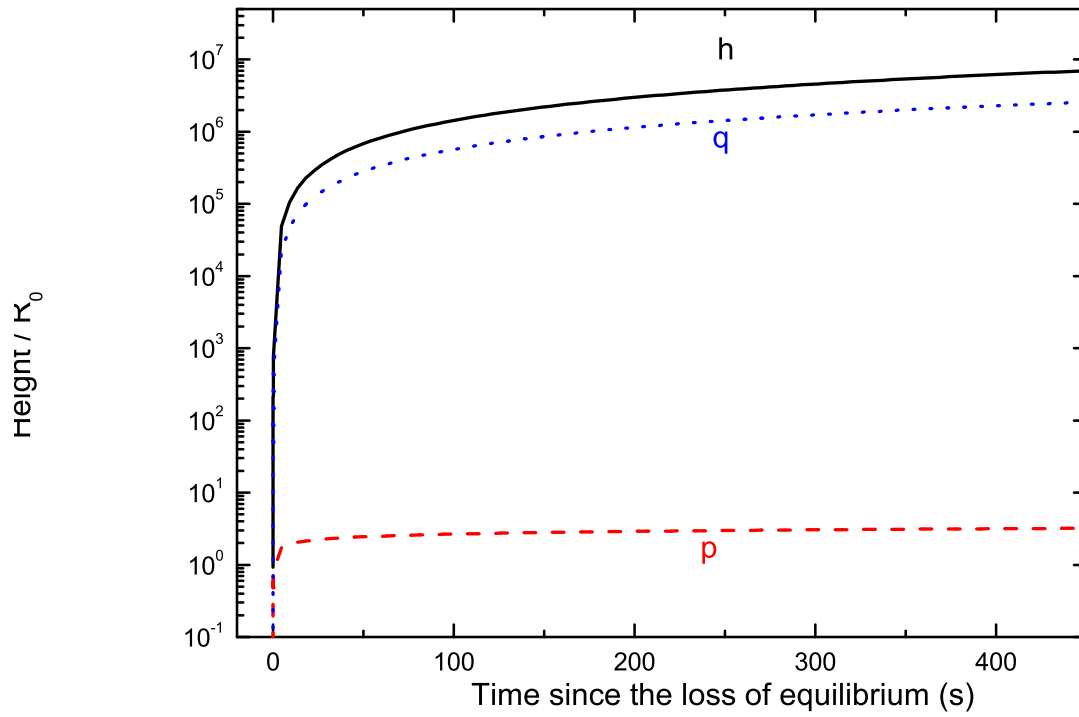


Fig. 4.— Plots of the height of the flux rope, h , and the top and the bottom tips of the current sheet (q, p) as function of time.

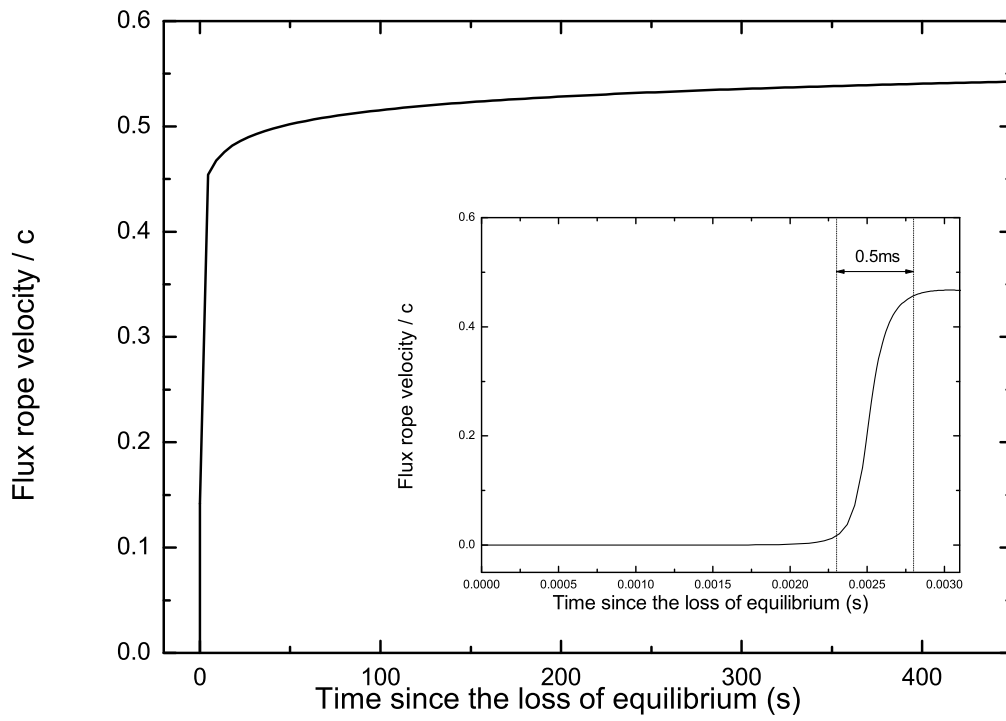


Fig. 5.— Plots of the velocity of the flux rope as a function of time. The inset describes the detailed evolution in the speed of the flux rope, which implies a very energetic eruption.

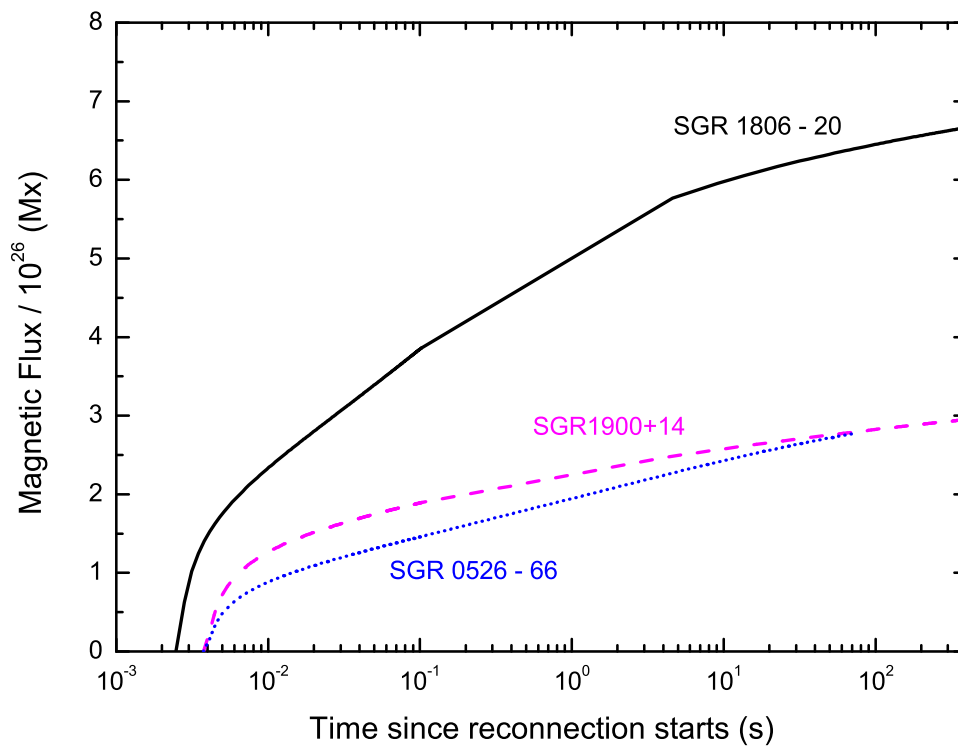


Fig. 6.— Variations of the total magnetic flux sent into interstellar space by reconnection versus time for three giant flares occurring on different magnetars.

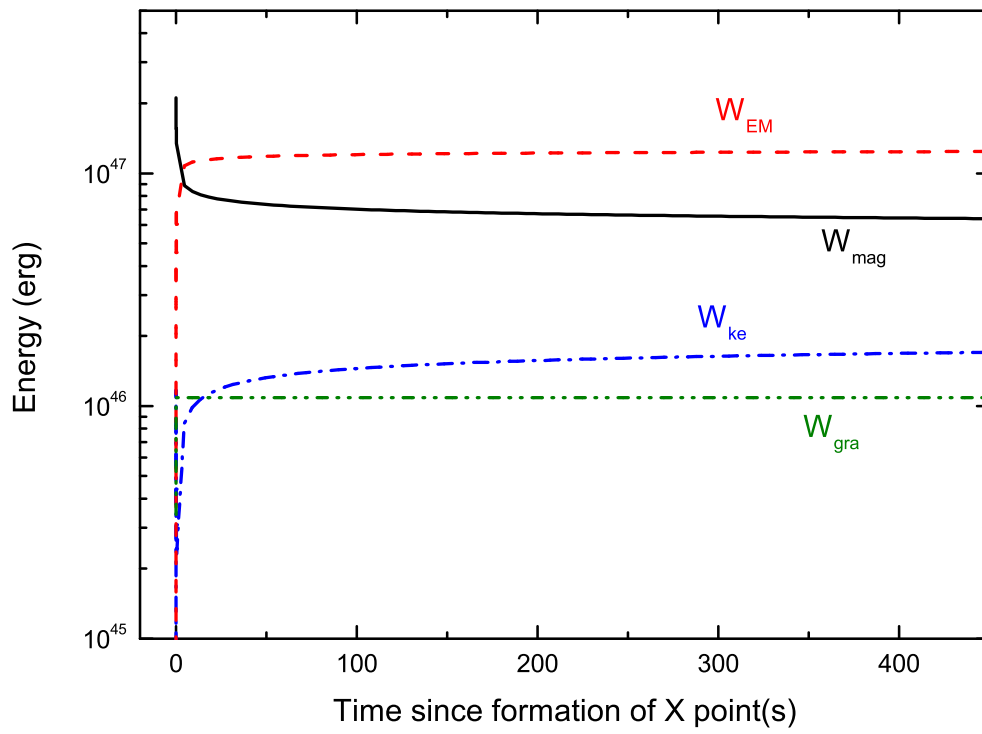


Fig. 7.— Plots of magnetic energy W_{mag} , radiative energy W_{EM} , gravitational energy W_{gra} and kinetic energy W_{ke} as function of time for SGR 1806-20.

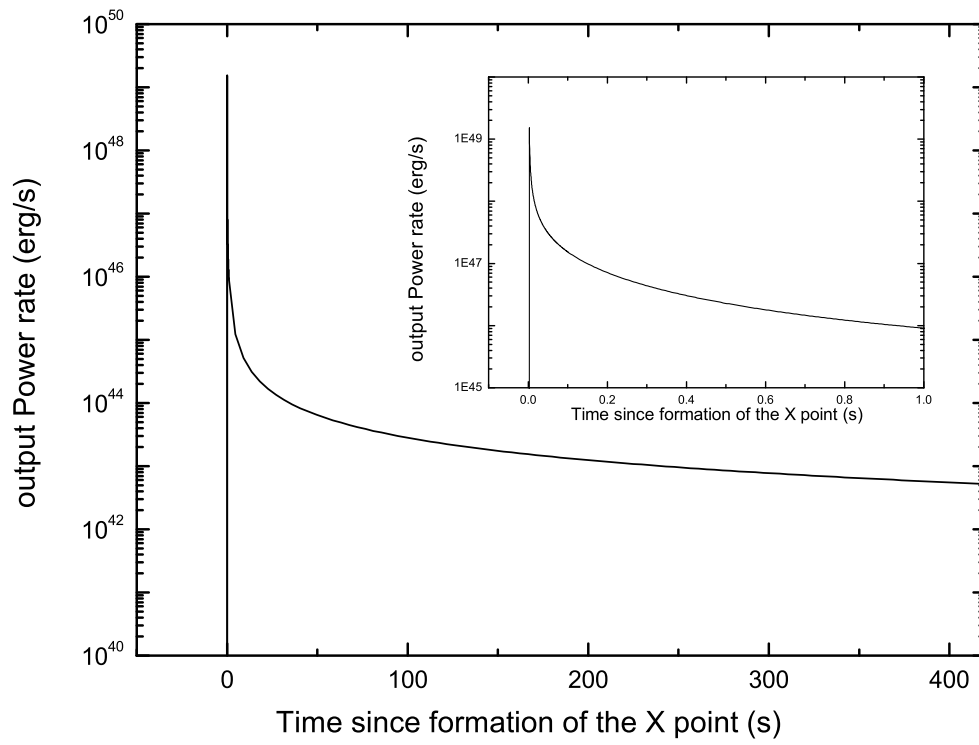


Fig. 8.— Light curve of the eruption governed by $S(t)$ given in equation (12).

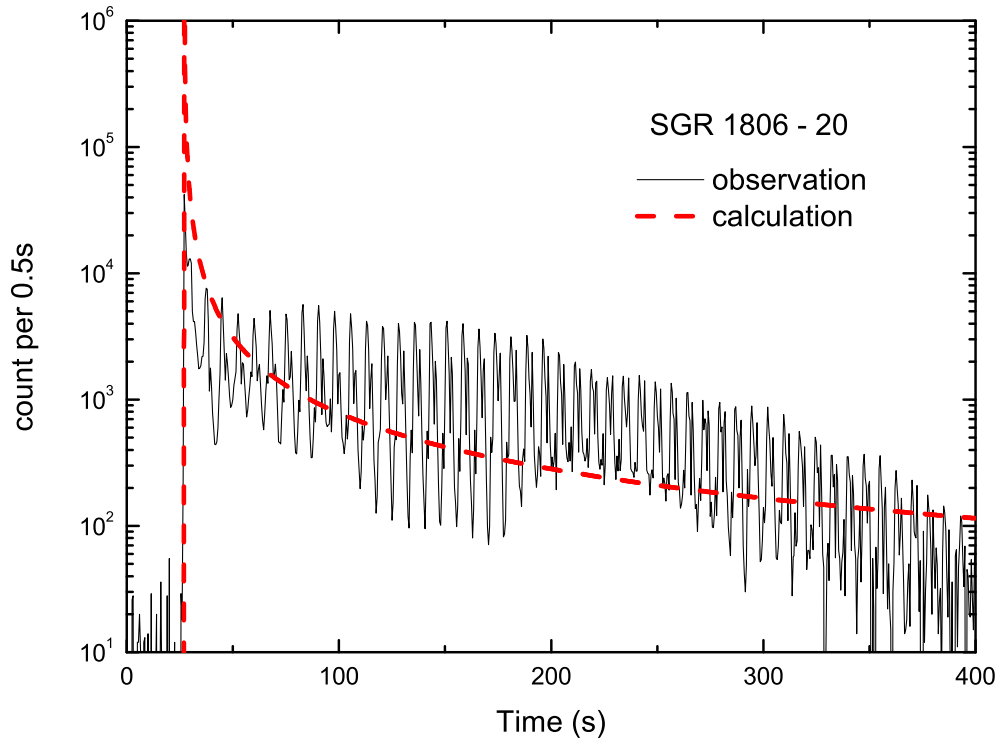


Fig. 9.— Light curve for the SGR 1806-20 giant flare given by calculations compared with the observations from the RHESSI spacecraft.

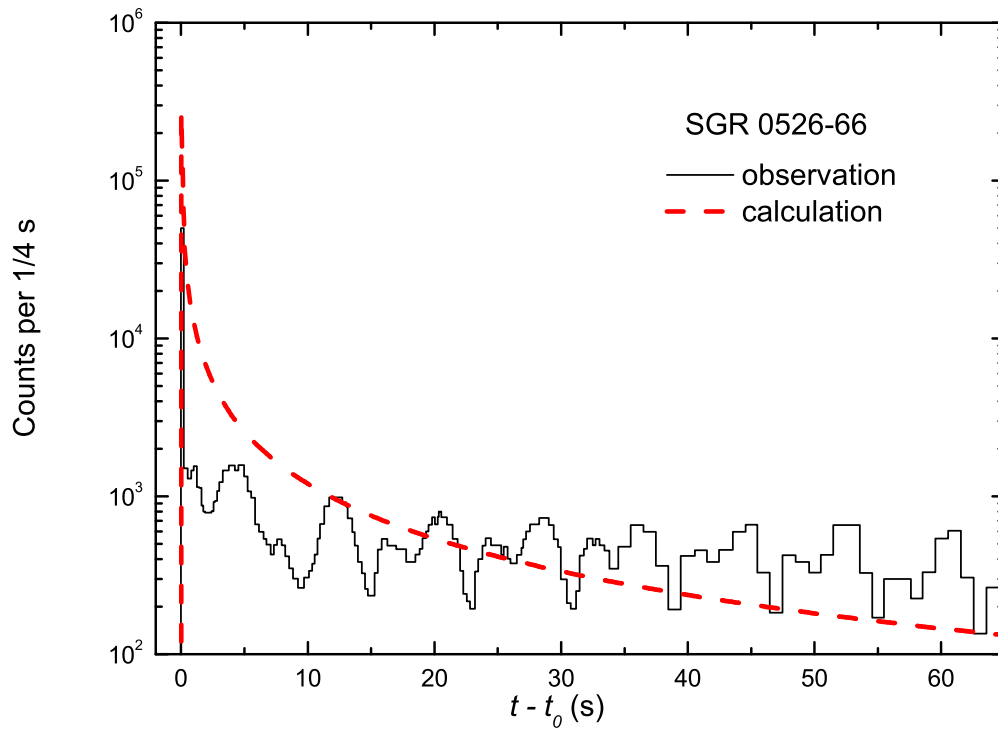


Fig. 10.— Light curve for the SGR 0526-66 given by calculations compared with the observations from the Venera spacecraft.

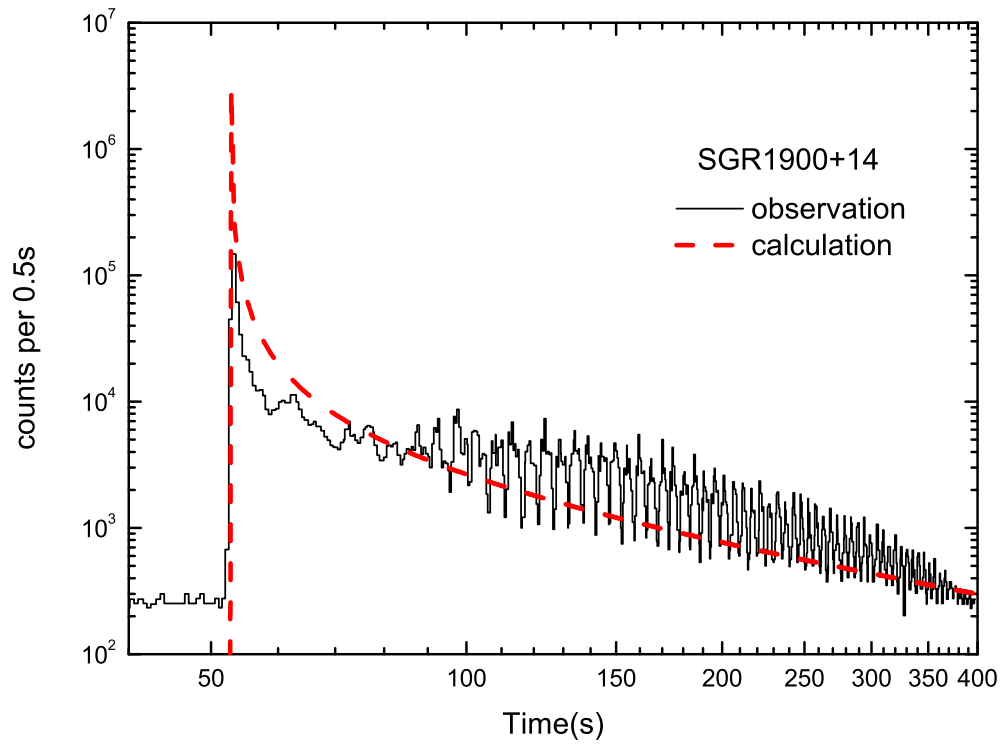


Fig. 11.— Light curve for the SGR 1900+14 given by calculations compared with the observations from the Ulysses spacecraft.